



Many competing ceria (110) oxygen vacancy structures: From small to large supercells

Jolla Kullgren, Kersti Hermansson, and Christopher Castleton

Citation: *J. Chem. Phys.* **137**, 044705 (2012); doi: 10.1063/1.4723867

View online: <http://dx.doi.org/10.1063/1.4723867>

View Table of Contents: <http://jcp.aip.org/resource/1/JCPSA6/v137/i4>

Published by the [American Institute of Physics](http://www.aip.org).

Additional information on *J. Chem. Phys.*

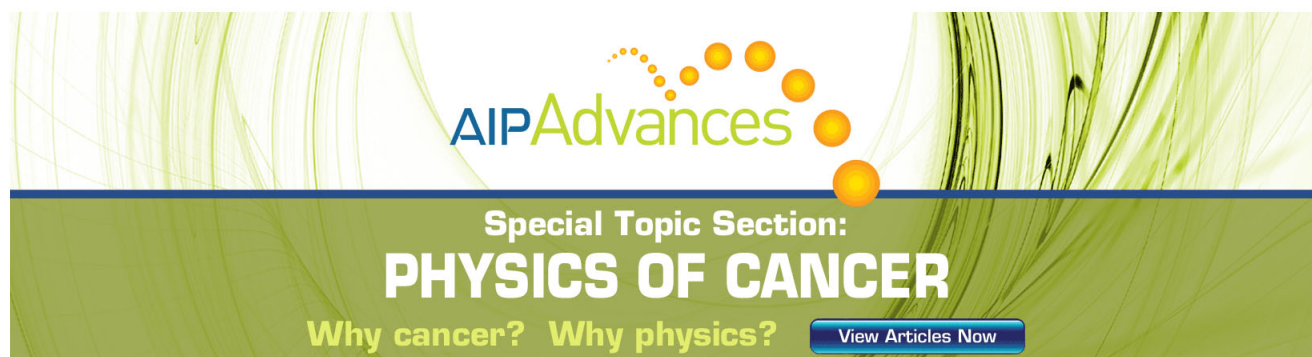
Journal Homepage: <http://jcp.aip.org/>

Journal Information: http://jcp.aip.org/about/about_the_journal

Top downloads: http://jcp.aip.org/features/most_downloaded

Information for Authors: <http://jcp.aip.org/authors>

ADVERTISEMENT



AIPAdvances

Special Topic Section:
PHYSICS OF CANCER

Why cancer? Why physics? [View Articles Now](#)

Many competing ceria (110) oxygen vacancy structures: From small to large supercells

Jolla Kullgren,¹ Kersti Hermansson,^{1,2} and Christopher Castleton³

¹*Department of Chemistry, The Ångström Laboratory, Uppsala University, Box 538, S-751 21, Uppsala, Sweden*

²*Department of Theoretical Chemistry, The Royal Institute of Technology (KTH), Roslagstullsbacken 15, S-106 91 Stockholm, Sweden*

³*School of Science and Technology, Nottingham Trent University, Nottingham NG11 8NS, United Kingdom*

(Received 31 August 2011; accepted 15 May 2012; published online 24 July 2012)

We present periodic “DFT+U” studies of single oxygen vacancies on the CeO₂(110) surface using a number of different supercells, finding a range of different local minimum structures for the vacancy and its two accompanying Ce(III) ions. We find three different geometrical structures in combination with a variety of different Ce(III) localization patterns, several of which have not been studied before. The desired trapping of electrons was achieved in a two-stage optimization procedure. We find that the surface oxygen nearest to the vacancy either moves within the plane towards the vacancy, or rises out of the surface into either a symmetric or an unsymmetric bridge structure. Results are shown in seven slab geometry supercells, $p(2 \times 1)$, $p(2 \times 2)$, $p(2 \times 3)$, $p(3 \times 2)$, $p(2 \times 4)$, $p(4 \times 2)$, and $p(3 \times 3)$, and indicate that the choice of supercell can affect the results qualitatively and quantitatively. An unsymmetric bridge structure with one nearest and one next-nearest neighbour Ce(III) ion (a combination of localizations not previously found) is the ground state in all (but one) of the supercells studied here, and the relative stability of other structures depends strongly on supercell size. Within any one supercell the formation energies of the different vacancy structures differ by up to 0.5 eV, but the *same* structure can vary by up to ~ 1 eV *between* supercells. Furthermore, finite size scaling suggests that the remaining errors (compared to still larger supercells) can also be ~ 1 eV for some vacancy structures. © 2012 American Institute of Physics. [<http://dx.doi.org/10.1063/1.4723867>]

I. INTRODUCTION

The character and roles of defects in metal oxides and other semiconductors are extremely important, with applications ranging from electronics to heterogeneous catalysis to future energy systems. One of the most popular computational approaches to studying such defects uses quantum mechanical calculations within the supercell approximation, together with plane waves, real space grids, or atomic basis sets, at theory levels from Hartree-Fock (HF) or density functional theory (DFT) and upwards. In the supercell approximation, a small block of atoms is surrounded by an infinite 1-, 2-, or (most commonly) 3-dimensional array of copies of itself using periodic boundary conditions (PBCs). This has both algorithmic and modelling advantages, but does introduce errors in the description of isolated defect properties, which we will examine in this paper for the case of an oxygen vacancy on the (110) surface of ceria.

Oxygen vacancies in ceria, particularly at the (111) and (110) surfaces, play a significant role for ceria's catalytic properties, oxygen storage capacity and use in solid oxide fuel cells. In all of these, the vacancy structures, formation energies, and diffusion barriers are very important. So far, most experimental,¹⁻⁶ and many theoretical⁶⁻¹⁰ studies have considered vacancies only on the (111) surface of ceria, since experimentally this is normally the most stable, and theoretical studies using analytical force-fields (FF),¹¹⁻¹⁵ HF,¹⁶ and DFT¹⁷⁻²⁴ all essentially support the experimental

findings and agree on the order of stability: (111) > (110) > (100). However, it has been suggested that much of the interesting surface chemistry may be taking place not on the most stable (111) surface, but rather on other surfaces or possibly at step-edges or at other topological surface defects. For example, Henderson *et al.* proposed that the reactivity of non-(111) terminations accounts for the oxidative behaviour of water on reduced powders.²⁵ As for the stability (and hence predicted concentration) of *surface oxygen vacancies*, studies with different types of DFT¹⁸⁻²⁰ (see also the review in Ref. 26) and FF methods¹¹⁻¹³ all agree that the stability actually follows the order: (110) > (100) > (111). In the current paper we will focus on the case of a single oxygen surface vacancy on the ceria(110) surface and the ionic and electronic reorganizations that it induces.

The cerium ions in pure ceria are (nominally) in the oxidation state Ce(IV), but the formation of neutral oxygen vacancies is believed to involve two cerium ions changing to Ce(III). Evidence is largely indirect, such as some x-ray and electron spectroscopic studies²⁷⁻²⁹ that indicate the presence of two distinct Ce ion species, nominally Ce(III) and Ce(IV). Further support comes from the non-band-like conductivity, which corresponds to thermally activated hopping of self-trapped Ce 4*f* electrons (polarons), and fits the “small polaron” model³⁰⁻³² of Holstein *et al.* This indicates that the polarons' linear dimensions are “of the order of the lattice spacing,” although not necessarily restricted purely to single Ce ions. Perhaps the best evidence for Ce(III) localization near

TABLE I. Predicted ground state structures for a single oxygen vacancy on ceria (110). The Method column lists in parentheses the value of the Hubbard parameter U and, when applicable, the type of pseudo-potential, viz. ultrasoft (US-PP) or projector-augmented-wave method (PAW). The abbreviations in the table stand for the following concepts and methods: LDA (local density approximation), PW91 (the Perdew and Wang functional), PBE (the Perdew, Burke, and Ernzerhof functional), ECP (effective core potential), FF (force-field), MD (molecular dynamics simulations).

Method	Loc. pattern	Supercell	Reference
Symmetric bridge (s-Bri)			
DFT-PW91 (PAW)	Delocalized	$p(2 \times 1)$, $p(2 \times 2)$	Yang <i>et al.</i> (2004) (Ref. 18)
FF-MD (shell model potential)	Not included	$p(4 \times 3)$	Gotte <i>et al.</i> (2004) (Ref. 34)
MP2 (local basis set with ECPs)	(1,2)	Ce ₁₀ O ₁₉ embedded cluster	Herschend <i>et al.</i> (2005) (Ref. 33)
Unsymmetric bridge (u-Bri)			
DFT-PBE+U ($U = 5$ eV, PAW)	(1,8)	$p(2 \times 2)$	Galea <i>et al.</i> (2009) (Ref. 35)
DFT-PBE+U ($U = 5$ eV, PAW)	(1,4)	$p(2 \times 2)$, $p(2 \times 3)$, $p(3 \times 2)$, $p(4 \times 2)$, $p(3 \times 3)$	This work (2012)
DFT-PBE+U ($U = 5$ eV, PAW)	(1,3)	$p(2 \times 4)$	This work (2012)
Symmetric in-plane (s-InPl)			
DFT-PW91+U ($U = 5$ eV, PAW)	(1,2)	$p(2 \times 1)$	Nolan <i>et al.</i> (2005) (Ref. 19)
DFT-PBE+U ($U = 4.5$ eV, US-PP)	(1,2)	$p(2 \times 1)$, $p(2 \times 2)$	Fabris <i>et al.</i> (2005) (Ref. 20)
DFT-LDA+U ($U = 5.3$ eV, US-PP)	(1,2)	$p(2 \times 1)$, $p(2 \times 2)$	Fabris <i>et al.</i> (2005) (Ref. 20)
DFT-PBE+U ($U = 5$ eV, PAW)	(1,2)	$p(2 \times 2)$	Yang <i>et al.</i> (2008) (Ref. 36)
DFT-PBE+U ($U = 5$ eV, PAW)	(1,2)	$p(3 \times 3)$	Yang <i>et al.</i> (2009) (Ref. 37)
DFT-PBE+U ($U = 5$ eV, PAW)	(1,2)	$p(2 \times 1)$	This work (2012)

vacancies comes from the combined STM and DFT study of vacancies on the (111) surface by Jerratsch *et al.*⁶ Reference 6 found that the two polarons are indeed confined to individual cerium ions and that at most one of these resides at an NN position relative to the vacancy. The latter result is in agreement with other DFT studies^{7–10} that had shown that the reduced cerium ions connected to (111) surface and subsurface vacancies are most stable at next-nearest neighbour (NNN) positions relative to the vacancies. We will show here that the so-called “standard picture” of localization at NN positions also fails for vacancies at the (110) surface.

Actually, for one O vacancy on the ceria(110) surface, even within the “standard” NN localization pattern, *three different geometrical structures* for the surface oxygen vacancy have been reported in the literature, but separately by different authors, which may explain why the existence of three competing geometric structures has so far been overlooked, and the difference between them consequently not noted or discussed; see Table I and Fig. 1. In the first structural type, which we hereafter denote *symmetric bridge* (s-Bri), an oxygen ion neighboring the oxygen vacancy moves “upwards” out of the surface layer, to occupy a bridging site, where it is coordinated *only* to the two top-layer cerium ions next to the vacancy. This oxygen ion, which moves so much as a result of the oxygen vacancy creation, is “the geminal oxygen” ion, shown and defined in Fig. 1. The s-Bri structure has been found in periodic DFT calculations with the PW91 functional,¹⁸ using embedded cluster calculations with second order Moller-Plesset many-body perturbation theory (MP2),³³ and in FF molecular dynamics (MD) simulations.³⁴ We denote the second vacancy structure as *unsymmetric bridge* (u-Bri). It is a distorted version of the s-Bri structure, with different Ce–O distances to the bridging oxygen, as will be listed in the Results section. In the pictures, such as Fig. 1, it would be difficult to discern a difference between the s-Bri and u-Bri structures, so only the s-Bri type has been indicated. This type of unsymmetric structure was found using DFT with the

PBE+U functional in Ref. 35. A very similar structure was presented for a Zr-doped ceria (110) surface by Yang *et al.*³⁶ In the third structure, the surface oxygen ion coordinated to the two cerium ions neighbouring the vacancy is again displaced towards the vacancy but this time moves less far, and remains within the plane of the surface layer; see Fig. 1(b). This *symmetrical in-plane* (s-InPl) structure has been found using DFT with LDA+U,²⁰ PW91+U¹⁹ and PBE+U.^{20,36,37}

In comparing the three structures in this paper, we find that a large part of the difficulty in identifying the relative stabilities of these vacancy structures is related to the choice of periodic supercells used for the calculations, which, as we will show, have often been too small to uniquely contain the various important different localization patterns. All but one of the DFT-based studies in Table I used only the $p(2 \times 1)$ and/or $p(2 \times 2)$ supercells, i.e., 2 or 4 repeats of the basic (110) surface unit cell. The remaining calculation³⁷ used $p(3 \times 3)$, finding an in-plane structure. (The classical force field calculations in Ref. 34 used the $p(4 \times 3)$ supercell.) A related difficulty concerns the errors that arise because the defects can interact (electrostatically, elastically, and quantum-mechanically³⁸) with their own mirror images in the periodic boundary conditions (see Refs. 39–42 for example). Even for those situations/applications where a certain supercell model corresponds to a realistic *concentration* of vacancies, the structure itself is rarely realistic, since a supercell corresponds to an ordered array of defects at some particular concentration, while real materials will more often be disordered, with regions in which defects are spread more widely apart, and other regions in which they are close neighbours. We will present calculations using the following cells: $p(2 \times 1)$, $p(2 \times 2)$, $p(2 \times 3)$, $p(3 \times 2)$, $p(2 \times 4)$, $p(4 \times 2)$, and $p(3 \times 3)$ supercells. This will allow us to estimate the scale of the supercell size errors and their potential impact on isolated vacancy stabilities and localization patterns (and in principle similar properties of defects in metal oxides in general).

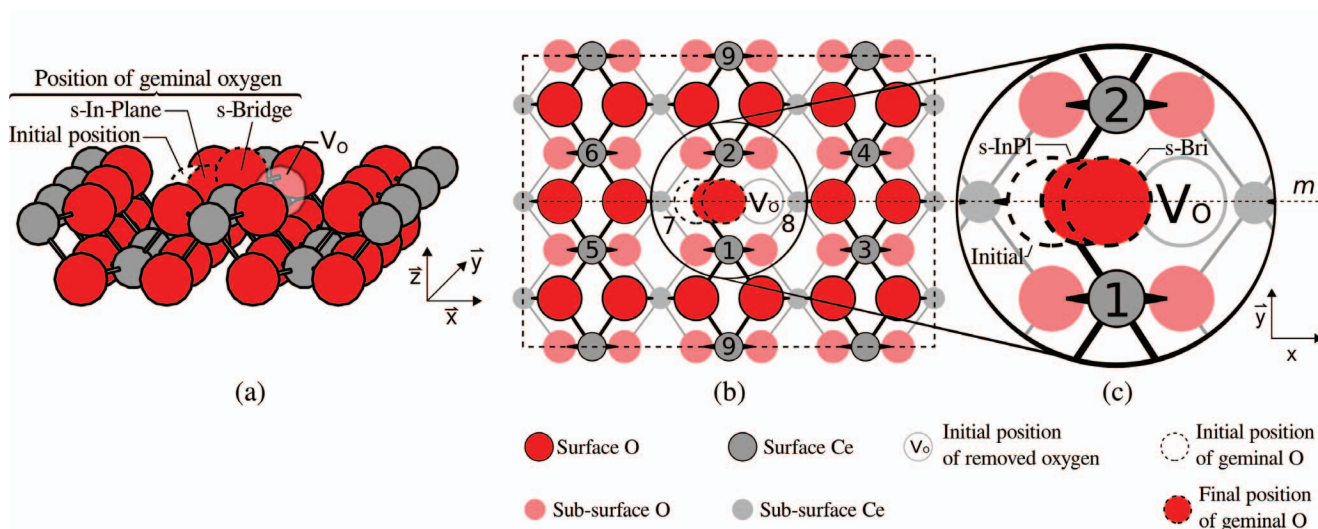


FIG. 1. A schematic representation of the relaxation around a single vacancy on the ceria (110) surface. The figure shows side view (a) and top view ((b) and (c)) of the symmetric in-plane (s-InPl) and symmetric bridge (s-Bri) structures. Here and in Fig. 2, gray circles represent cerium ions and oxygen are represented by red circles. V_O marks the initial position of the removed oxygen while the dashed circles represent the initial and final positions of the geminal oxygen for the InPl and s-Bri cases. The “geminal oxygen” is defined in (a) and means the remaining oxygen which, like the removed oxygen, coordinates to ceriums 1 and 2. In the unsymmetric bridge structure (u-Bri, not shown), the geminal oxygen tilts slightly out of the vertical mirror plane m and towards either cerium 1 or 2 (see Table II). The labels on the cerium ions are used for the description of the localization patterns in the text and tables. Note that Ce 9 occurs twice as it lies on the edge of the supercell.

Section II describes the model systems and the computational details. Here we also discuss our approach to steering the structural optimizations towards the desired location pattern. In Sec. III we will start by presenting results for the Ce4f electron localization patterns and vacancy structures in our largest supercell, $p(3 \times 3)$, before considering how this varies with supercell size in Sec. IV. In Sec. V we will conclude.

II. METHOD

A. Computational details

All DFT calculations in this study were performed using the Vienna *ab initio* simulation package (VASP).^{43,44} We have used the simplified rotationally invariant form of GGA+U ($U = 5$ eV) due to Dudarev *et al.*⁴⁵ as implemented in the VASP code. In this study, we used the GGA (generalized gradient approximation) functional PBE developed by Perdew *et al.*⁴⁶ The DFT+U (LDA+U and GGA+U) methods have been shown to overcome the inability of LDA and GGA to describe the localized Ce4f electrons in ceria with reduced cerium ions.^{21,22} The choice of the U parameter value was explored in several previous studies^{21,47–50} and it has been noted (Ref. 50 and elsewhere) that LDA+U actually provides a better overall description of ceria than GGA+U. However, we will keep to GGA+U in the present study, in order to maintain compatibility and comparability with previous studies of vacancies on ceria (110) (cf. Table I).

For the cerium and oxygen ions, 12 and 6 electrons, respectively, are attributed to the valence space. The remaining core electrons are treated with the projector augmented wave (PAW) method of Blöchl.⁵¹ For all calculations an energy cutoff of 408 eV was used for the plane-wave basis and integrations over the Brillouin zone were done using a Gaussian smearing of 0.2 eV. Tests were also done with a smearing

of 0.05 eV, and it was found that calculated defect energies changed by only around 0.002 eV. The Brillouin zone itself was sampled using a $2 \times 4 \times 1$ grid for the $p(2 \times 1)$ supercell, and a $2 \times 2 \times 1$ grid for the $p(2 \times 2)$, $p(2 \times 3)$, $p(3 \times 2)$ and $p(3 \times 3)$ supercells. Finally, a $2 \times 1 \times 1$ and a $1 \times 2 \times 1$ grid was used for the $p(2 \times 4)$ and $p(4 \times 2)$ supercells, respectively. (Note: A consistent set of k-point samplings based on, say, $6 \times 12 \times 1$ in $p(2 \times 1)$ would be possible, but would be computationally excessive. For example, in $p(2 \times 1)$ the difference in energy would be less than 1 meV.)

We present structures (i.e., geometric structures and electron localization patterns) and formation energies. The structures were obtained by optimizing the total energy, stopping when forces on all atoms were less than 0.01 eV/Å. All vacancy structures were relaxed in a two stage process, in order to help trap electrons at specific targeted positions. In the first relaxation stage, a different cerium PAW potential was used for the two targeted cerium ions, in which the Ce4f electron was assigned to the core. The first stage result was then used as a start point for further relaxation in the second. Here, all cerium ions were described using the regular PAW potential, with all Ce4f electrons treated as valence, so that localization patterns can change if the targeted one is not a local minimum after all.

The formation energy E_{vac} is obtained from the equation

$$E_{vac} = E^T(\text{CeO}_{2-x}) - \left[E^T(\text{CeO}_2) - \frac{1}{2} E(\text{O}_2(g)) \right], \quad (1)$$

where $E^T(\text{CeO}_{2-x})$ and $E^T(\text{CeO}_2)$ are the total energy of the optimized supercell with and without the vacancy, calculated using the same values of plane-wave cutoff, k-point grid, etc, to make use of the cancellation of errors. $E(\text{O}_2(g))$ is the energy of an oxygen dimer.

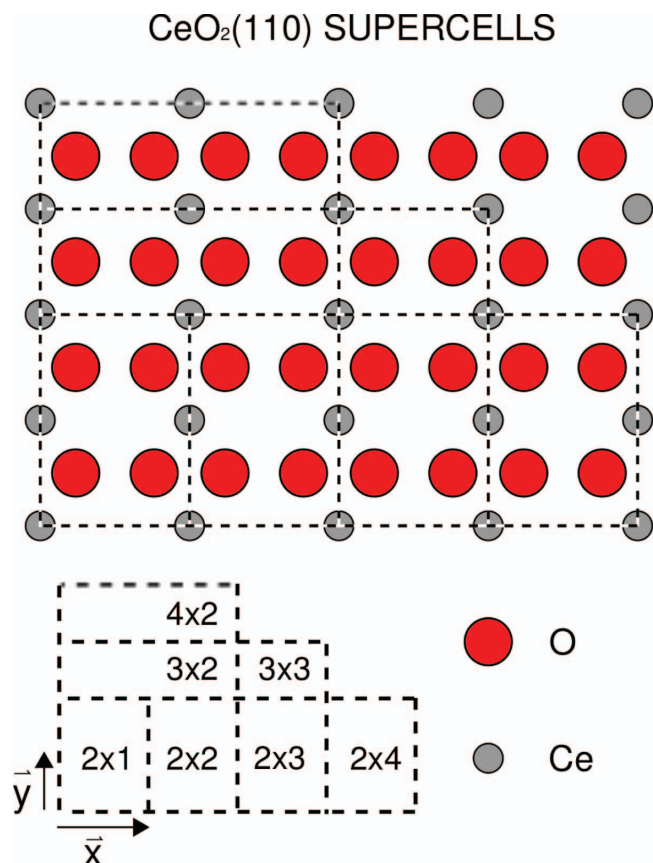


FIG. 2. A schematic representation of the seven different supercells used in this study. The figure shows a top view of the top most layer in the supercell.

It should be noted that the absolute values reported here for E_{vac} thus depend on the description of the oxygen dimer, which is in general only poorly described by plane-wave DFT using GGA or LDA. However, we are mostly concerned here with relative energies, which are unaffected by errors in the oxygen dimer energy. We will use the value of -9.41 eV for the energy of the optimized oxygen dimer, obtained by fitting a quadratic curve to an energy versus O–O separation.

B. Model systems

As mentioned in the Introduction, single oxygen vacancies on the ceria (110) surface are modeled here using seven different supercells, namely, $p(2 \times 1)$, $p(2 \times 2)$, $p(2 \times 3)$, $p(3 \times 2)$, $p(2 \times 4)$, $p(4 \times 2)$, and $p(3 \times 3)$, see Fig. 2. All of the systems were constructed as slabs separated by a large vacuum gap. The vacuum gap was ~ 15 Å in the z -direction and all systems had a horizontal mirror plane passing through the center of the slab, i.e., parallel to the surface. The coordinates of the atoms in the horizontal mirror-plane were kept fixed in all calculations, and this mirror symmetry was maintained in all calculations. All slabs had a thickness of 7 atomic layers (≈ 12 Å). Tests were performed with slabs with 5 and 9 atomic layers. The surface energy, E_{surf} , was calculated for the 5-, 7- and 9-layer slabs using the formula

$$E_{surf} = \frac{1}{S} (E_{slab,N}^T - E_{bulk,N}^T), \quad (2)$$

where $E_{slab,N}^T$ is the energy of the slab supercell, $E_{bulk,N}^T$ is the energy of a bulk cell containing the same number of formula units (N) as the slab supercell and S is the surface area of the slab supercell counting both faces.

Our surface energy is 1.1 J/m² for the stoichiometric 9-layer slab and in line with previous studies (HF,¹⁶ LDA,¹⁷ PW91,¹⁷ and GGA+U (Ref. 22)) we find the surface rumpling to be 0.14 Å, with top layer cerium ions displaced towards the center of the slab relative to oxygen ions. The difference in surface energy between the 7- and 9-layer slabs is less than 0.01 J/m².

The spatial dimensions of the bounding box in the x - and y -directions (the $[001]$ and $[1\bar{1}0]$ directions, respectively) were fixed at the optimized cell parameter of the cubic CeO₂ structure obtained from a bulk calculation using the same functional (PBE+U). In the z direction ($[110]$ direction) the supercell parameter was fixed at 27.0 Å.

Note: In the $p(2 \times 1)$ system, all surface cerium ions are formally Ce(III), and the vacancies can hardly be considered to be isolated. However, it is included for comparison since several of the previous studies used this supercell.^{18–20,23}

Next we will present our results.

III. RESULTS FOR Ce(III) CONFIGURATIONS AND VACANCY STRUCTURES IN THE $p(3 \times 3)$ CELL

We will use the $p(3 \times 3)$ supercell to investigate the stability of 9 different localization patterns, or localization “configurations,” for the single vacancy at the ceria (110) surface. These different localization patterns represent unique pair combinations among the 9 cerium ions marked in Fig. 1: (1,2), (1,3), (1,4), (1,8), (3,4), (3,5), (3,6), (7,8), and (4,9). Other configurations such as (1,7), (1,6), and (1,5) would, in principle, be possible. However, these structures actually become equivalent to configurations (1,8), (1,4), and (1,3) after relaxation. The movement of the geminal oxygen effectively splits the vacancy over two positions, so in the following, NN and NNN will refer to the Ce(III) positions relative to the effective centre of mass of the vacancy, which is under the relaxed position of the geminal oxygen for s-Bri, and close by for u-Bri and InPl, rather than referring to the original vacancy position. The difference is only slight, but it gives a more intuitive and practical definition, and is used, for example, in the second column of Table II.

We find only one configuration that gives rise to an in-plane (InPl) structure, namely (1,2). In this configuration, the excess electrons localize on the two cerium ions closest to the vacancy (Cerium ions 1 and 2 in Fig. 1). Symmetric structures (s-Bri) are found for localization on the pairs (1,2), (3,4), (3,6), and (7,8). Similarly, unsymmetric bridge (u-Bri) structures are found for localization on the pairs (1,3), (1,4), (4,9), and (1,8). In other words, if the localization pattern maintains the vertical mirror plane symmetry labelled m in Fig. 1, so does the geometrical structure of the vacancy. The exception is the (3,6) configuration which instead has a vertical C_2 rotational axis passing through the bridging oxygen. Moreover, only for the (1,2) configuration do we find that two different structural minima are possible: the s-Bri and the In-Pl structures; the latter is slightly more stable (Table II). Note that, in the following, subscripts are sometimes added to the labels

TABLE II. Vacancy formation energies, E_{vac} , and selected interatomic distances for different electron localization configurations and geometrical structures (s-Bri, u-Bri, s-InPl) optimized for a single oxygen vacancy on the ceria (110) surface using a $p(3 \times 3)$ supercell. The notation is as follows. *The first column* (labelling scheme as described in the text), *second column* (the locations of the Ce(III) ions, sub-NN refers to the second atomic layer, otherwise it is the top layer), *third column* (E_{vac}), *fourth column* (resulting distances between the geminal oxygen and Ce₁ and Ce₂), *columns 5–6* (resulting interatomic distance involving the two Ce(III) ions), *column 7* (the vertical displacement of the geminal oxygen compared to the relaxed O ion at the stoichiometric surface).

Label	Localization pattern	E_{vac} (eV)	$O_{gem}-Ce_1, O_{gem}-Ce_2$	$O_{gem}-Ce^{3+}$	$Ce^{3+}-Ce^{3+}$	$\delta z O_{gem}$
Symmetric bridge (s-Bri)						
s-Bri ₁₊₂	(1,2) NN, NN	1.98	2.22, 2.22	2.22, 2.22	4.21	0.77
s-Bri ₃₊₄	(3,4) NNN, NNN	1.89	2.22, 2.22	5.89, 5.89	3.91	0.51
s-Bri ₃₊₆	(3,6) NNN, NNN	1.59	2.22, 2.22	5.82, 5.85	6.74	0.52
s-Bri ₇₊₈	(7,8) sub-NN, sub-NN	1.95	2.23, 2.23	3.69, 3.61	5.61	0.41
Unsymmetric bridge (u-Bri)						
u-Bri ₁₊₃	(1,3) NN, NNN	1.58	2.36, 2.09	2.36, 5.94	5.48	0.67
u-Bri ₁₊₄	(1,4) NN, NNN	1.54	2.36, 2.09	2.36, 5.80	6.78	0.66
u-Bri ₁₊₈	(1,8) NN, sub-NN	1.77	2.36, 2.10	2.36, 3.56	3.99	0.56
u-Bri ₃₊₅	(3,5) NNN, NNN	1.59	2.23, 2.21	2.21, 5.82	5.52	0.52
u-Bri ₄₊₉	(4,9) NNN, NNN	1.68	2.20, 2.21	5.85, 5.87	6.69	0.57
Symmetric in-plane (s-InPl)						
s-InPl ₁₊₂	(1,2) NN, NN	1.91	2.33, 2.33	2.33, 2.33	4.26	0.02

s-Bri, u-Bri, and InPl. These subscripts refer to the positions of the two Ce(III) ions according to Fig. 1.

The vacancy formation energies of the different structures are collected in Table II, together with selected interatomic distances and the vertical or upwards displacement (perpendicular to the surface) of the bridging oxygen. The horizontal distance of the geminal oxygen perpendicular to the cerium bridge is less than 0.07 Å for all structures except u-Bri₁₊₈ where it is about 0.2 Å.

Like Galea *et al.*,³⁵ we find that the most stable vacancy structure is an u-Bri structure. However, the u-Bri structure with the localization pattern that Galea *et al.* found, u-Bri₁₊₈, where the two additional Ce4f electrons are located at one NN surface cerium (Cerium 1 in Fig. 1) and one NN sub-surface cerium (cerium 8 in Fig. 1) is not the most stable one in our calculations. Instead, we find that u-Bri₁₊₄ is the most stable; here only Cerium ions at the surface are involved, namely, one NN and one NNN ion. The u-Bri₁₊₄ structure has a vacancy formation energy of 1.54 eV, compared to 1.77 eV for u-Bri₁₊₈. The tendency for the oxygen vacancy to coordinate Ce⁴⁺ has also been observed for the (111) surface^{7,10} and similarly for Ti⁴⁺ at the TiO₂ (110) rutile surface in the work by Deskins *et al.*⁵² Ce4f localization at NNN positions appears to emerge as a compromise between competing effects. On the one hand, pure electrostatics prevents the Ce³⁺ charge from localizing far from the vacancy, while, on the other hand, the closer neighbour positions (especially NN) are disfavoured due to complications in local relaxation, such as the larger size of the Ce³⁺ ion relative to the Ce⁴⁺. As Table II shows, the near degeneracy ($\delta E < 0.1$ eV) between structures with localization at only NNN positions [e.g., (3,6)] and those with localization at one NN and one NNN [e.g., (1,4)] is similar to that observed on the (111) surface.¹⁰ The difference is that while the pure NNN configurations seem to be the ground state on the (111) surface the mixed situation seems to be the ground state here on the (110). However, we will see in Sec. IV that the pure NNN structure could in fact be the ground state in the the infinite supercell size limit.

Deskins *et al.*⁵² observed a similar complexity in the distribution of excess electrons for TiO₂ and demonstrated that the polaron-polaron interaction is much weaker than the polaron-vacancy interaction. Such a result can be used to substantially reduce the number of calculations needed in order to establish the ground state distribution of excess electrons and could certainly be an interesting approach for future studies of oxygen vacancies at the CeO₂ (110) surface.

For a *bulk vacancy* in a similarly sized supercell (specifically, a $2 \times 2 \times 2$ multiple of the crystallographic unit cell) we find a formation energy of 3.22 eV. For this bulk cell we considered configurations where the excess electrons are either at two NN cerium ions with respect to the vacancy or at two NNN cerium ions. There are four unique localizations of the NNN+NNN type. We find basically the same energy regardless of the localization configuration, with energies in the range 3.22–3.31 eV, and the smallest value occurring for one of the NNN+NNN localizations. This suggests that there will be a significant tendency for vacancies in the bulk of ceria to migrate to the surface, at least at low temperature, and conversely significant barriers to diffusion of vacancies away from the surface. Defect segregation of this type is quite common (see Refs. 53–55 for example). It should be noted, however, that we have omitted all entropy contributions in our discussion, since they are extremely difficult to either calculate or estimate. At high temperatures these can dominate, and it is plausible that they then will favour vacancy diffusion back into the bulk.

IV. RESULTS FOR DEPENDENCE ON SUPERCELL SIZE

In order to study the effect of supercell size on our results, we have repeated most of the calculations using six smaller supercells. It is not possible to explore all of the localizations considered above in all of the supercells, as some are too small. We have instead chosen the 6 structures that can, in principle, fit into supercells from $p(2 \times 2)$ and upwards (Table III).

TABLE III. Vacancy formation energies E_{vac} for various vacancy structures and Ce4f localization patterns in the seven supercells considered. Six of the ten cases from Table II are listed (see text). p(2×2) is entered three times for clarity of comparison.

Supercell	s-InPl ₁₊₂	s-Bri ₁₊₂	s-Bri ₃₊₄	u-Bri ₁₊₃	u-Bri ₁₊₄	u-Bri ₁₊₈
p(2 × 1)	2.31	2.84	2.48
p(2 × 2)	2.23	2.39	2.05	1.77	1.74	2.03
p(2 × 3)	2.22	2.28	2.30	1.77	1.76	1.97
p(2 × 4)	2.22	2.29	2.32	1.77	1.78	1.96
p(2 × 2)	2.23	2.39	2.05	1.77	1.74	2.03
p(3 × 2)	1.94	2.01	1.72	1.59	1.56	1.74
p(4 × 2)	1.85	1.87	1.55	1.52	1.51	1.66
p(2 × 2)	2.23	2.39	2.05	1.77	1.74	2.03
p(3 × 3)	1.91	1.98	1.89	1.58	1.54	1.77

We find that all six of these structures are stable in each of the additional six supercells. However, the formation energy can vary by up to 0.97 eV for one and the same vacancy structure between the different supercells, as shown in Table III. Even omitting both the p(2 × 1) and p(2 × 2) supercells, the variation is up to 0.77 eV, which is a very significant variation. In contrast, the difference in energy between the various different structures as calculated within a *single* supercell is never more than 0.54 eV. Hence, the largest uncertainty in the vacancy formation energy values comes not from the variation between different localization patterns and structures, but from the choice of supercell.

The p(3 × 3) results were discussed in Section III, where the u-Bri₁₊₄ and u-Bri₁₊₃ were found to be the most stable vacancy structures. Here we find that they are the most stable in all supercells, except p(2 × 1), where it cannot exist. In p(2 × 1) the most stable structure is InPl with a (1,2) localization (s-InPl₁₊₂). For all the other supercells studied, the u-Bri₁₊₄ and u-Bri₁₊₃ structures are more-or-less degenerate, lying within 0.04 eV of one another; u-Bri₁₊₄ is the lowest in energy in all cells except p(2 × 4).

Our largest supercells here are still quite small and correspond to rather high defect concentrations. As mentioned in Sec. I, even for those situations/applications where such concentrations are realistic these ordered supercell structures are rarely so. Consequently, in defect studies we are not normally interested in the results from a specific supercell, but would rather want to know the stabilities and structures of lone defects, or equivalently, defects in infinitely large supercells or clusters. For defects in bulk supercells there has been much discussion about how to deal with, and correct for, the errors (relative to lone defects) introduced by the supercell approximation (see Refs. 40–42 and 56, for example). It has been shown that these errors can be estimated by scaling the formation energies from individual supercells with the inverse of the linear dimension ($\sim L$) and fitting to a polynomial in ($\sim \frac{1}{L}$) and $\sim \frac{1}{L^3}$ (Refs. 38 and 39), i.e., the leading error terms are inversely proportional to cell length and cell volume. To date, little has been done to extend this to defects on surfaces. The leading term may still be expected to be linear, but there is no *a priori* reason to assume that the next most important contribution scales as $\frac{1}{L^3}$ rather than, say, $\frac{1}{L^2}$.

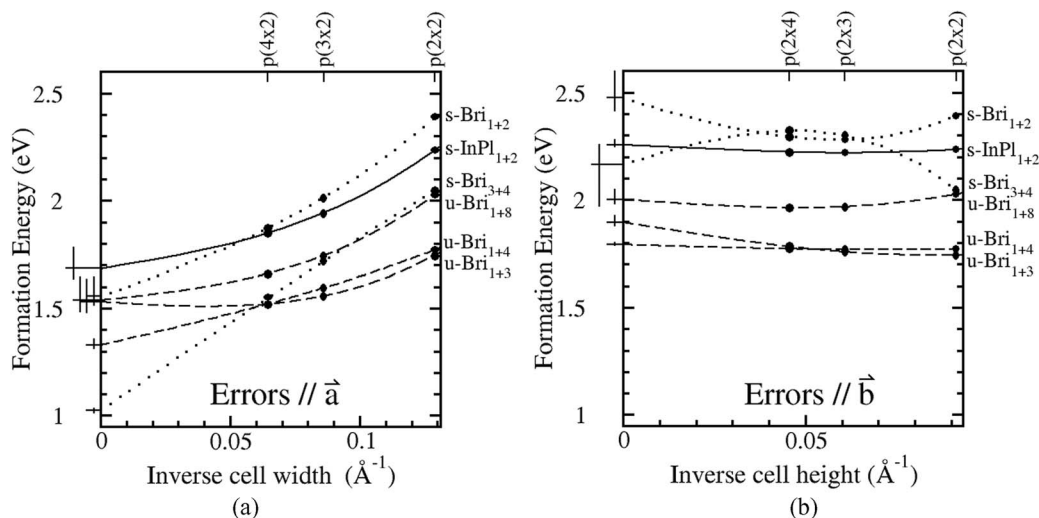


FIG. 3. Partial finite size scaling of formation energies with respect to inverse supercell size along the x-direction (a) and along the y-direction (b) for six types of oxygen vacancies on the CeO₂(110) surface. The fitting scheme and error bars are demonstrated and defined in Fig. 4 for the example of the x axis scaling of s-Bri₁₊₂.

TABLE IV. Formation energies, E_{vac} , for a single oxygen surface vacancy in the $p(2 \times 2)$ surface supercell and the extrapolated E_{vac} values along the x-direction ($p(\infty \times 2)$) and y-direction ($p(2 \times \infty)$). The scaling used is $1/L + 1/L^3$. Error bars are obtained by replacing $1/L^3$ with $1/L^2$ or with $1/L^4$ (see text). In the final line, x and y errors are combined to provide a speculative indication of where the lone vacancy formation energies may be. All energies in eV.

E_{vac} for diff. cells	s-InPl ₁₊₂	s-Bri ₁₊₂	s-Bri ₃₊₄	u-Bri ₁₊₃	u-Bri ₁₊₄	u-Bri ₁₊₈
$p(2 \times 2)$	2.23	2.39	2.05	1.77	1.74	2.03
$p(\infty \times 2)$	1.68 ± 0.10	1.55 ± 0.09	1.03 ± 0.01	1.33 ± 0.03	1.53 ± 0.10	1.54 ± 0.11
$p(2 \times \infty)$	2.26 ± 0.02	2.47 ± 0.12	2.17 ± 0.19	1.79 ± 0.01	1.89 ± 0.03	2.00 ± 0.05
$ p(\infty \times 2) - p(2 \times 2) $	0.55	0.84	1.02	0.44	0.21	0.49
$ p(2 \times \infty) - p(2 \times 2) $	0.03	0.08	0.12	0.02	0.15	0.03
$p(\infty \times \infty)$ estimated	1.71	1.63	1.15	1.35	1.68	1.57

or $\frac{1}{L^4}$. Second, the numerical values of the $\frac{1}{L}$ and $\frac{1}{L^n}$ coefficients are dependent upon the shape of the supercell used. In other words, if we had results here for, say, the series $p(2 \times 2)$, $p(3 \times 3)$, $p(4 \times 4)$, ..., or for $p(2 \times 1)$, $p(4 \times 2)$, $p(6 \times 3)$, ..., or equivalent, then we could estimate E_{vac} for an isolated defect. Our currently available resources do not allow us to calculate this for either the $p(4 \times 4)$ or $p(6 \times 3)$ or any other large enough supercell to get such a series. As a result we are unable to properly estimate lone vacancy energies at this point. The best we can do is to estimate the magnitude of the remaining supercell approximation errors, by considering the errors due to defect-image interactions along the x- and y-directions separately.

In Fig. 3(a) we estimate the x-direction errors using the supercell series $p(2 \times 2)$, $p(3 \times 2)$ and $p(4 \times 2)$, while Fig. 3(b) shows the y-direction errors using the series $p(2 \times 2)$, $p(2 \times 3)$, and $p(2 \times 4)$. In each case, the $\frac{1}{L} \rightarrow 0$ limit gives the result of removing the error in question. The largest uncertainty in these estimates comes from our lack of knowledge of the correct scaling form. This is illustrated in Fig. 4 for the case of the x-direction scaling of the formation energy for s-Bri₁₊₂, where three fits are shown, which assume that the errors scale as $1/L$ and $1/L^2$ (dotted), $1/L$ and $1/L^3$ (solid), or $1/L$ and $1/L^4$ (dashed). (See Fig. 4 caption for specific fitting equations.) The $\frac{1}{L} \rightarrow 0$ formation energy obtained is shown

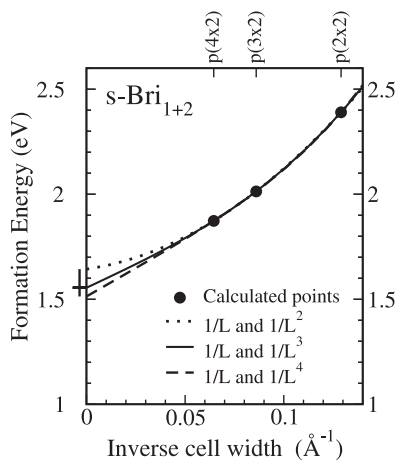


FIG. 4. Finite size scaling of formation energy with respect to inverse supercell size along the x axis for s-Bri₁₊₂. All three fits are performed to the equation $E_{vac}^C(L) = E_{vac}^\infty + a_1 L^{-1} + a_n L^{-n}$, where E_{vac}^C is the formation energy in supercell C , L is the cell width, and a_1 , a_n , and E_{vac}^∞ are fitting parameters, E_{vac}^∞ being the finite size scaled formation energy. The main fitted line (solid) assumes $n = 3$, while error bars are obtained from the alternative fittings: $n = 2$ (dotted line) and $n = 4$ (dashed line).

by the horizontal line to the left of the y axis, while the vertical line indicates the spread between these three candidate scalings. Such scaled energies and error bars are shown for all six defect structures in Figs. 3(a) and 3(b). The numerical values are shown in Table IV. For some structures, the effect of scaling up the supercell dimensions is relatively small (0.2–0.4 eV) but for others it is much larger, even around 1 eV or worse. This significantly affects the relative energies of the different structures, and suggests that a more complete scaling analysis, including data from still larger supercells, might find qualitative changes in the order and spacings of the stability of the various defect structures.

Note also that, in this particular case, errors arising due to defect-image interactions along the x-direction ([001]) are much more significant than those from interaction along the y-direction ($[1\bar{1}0]$). We can, in principle, add these two contributions together, as is done in the last line of Table IV. The result is startling: this estimate predicts that, in the lone defect limit, the most stable structure switches from u-Bri₁₊₄, which has one NN and one NNN Ce³⁺ ion, to s-Bri₃₊₄, which has two NNN Ce³⁺ ions and no NN ones. This is intriguing, not least in the context of recent work on the (111) surface,^{6,7,10} where NNN+NNN alone was also favoured. However, our results should be treated with caution since it is doubtful if errors due to defect-image interactions in the x- and y-directions can simply be added linearly in this way, and there is no clear way to establish how reliable (or otherwise) such a quantitative estimate is.

V. CONCLUSION

We have considered the effect of the choice of supercell on the results of periodic calculations for defects in metal oxides, through the specific example of the oxygen vacancy on the (110) surface of ceria. We have found three different local structures: symmetric and unsymmetric bridge type structures (s-Bri and u-Bri), in which an oxygen ion neighbouring the vacancy occupies a bridging position between the two surface layer cerium ions neighbouring the vacancy, and an in-plane type vacancy structure (In-Pl), in which the same oxygen neighbour moves towards the vacancy, but remains in the surface plane. Based on these three structures we have found nine different stable electron localization patterns in the $p(3 \times 3)$ supercell, with different positions for the two Ce(III) ions formed when the vacancy is created. The most stable structure in the $p(3 \times 3)$ cell is u-Bri with Ce4f electrons localized at the cerium

ions labelled 1 and 4 in Fig. 1: the u-Bri₁₊₄ structure. Here, cerium ion 4 is not a NN to the vacancy. This result for the (110) surface mirrors the previously reported tendency for oxygen vacancies to coordinate Ce⁴⁺ rather than Ce³⁺ on the ceria (111) surface.^{6,7,10}

The existence of several different low-lying structures may be significant for surface chemistry, since, for example, the reactivity of catalytically active sites does not only depend on their energy but also on their geometrical shape. Steric effects are indeed important in chemical reactions and knowing the relevant structures of the vacancies is therefore important when designing models for, say, a catalytic reaction step.

We have repeated our calculations for the six “smallest” defect structures in the seven supercells p(2 × 1), p(2 × 2), p(2 × 3), p(3 × 2), p(3 × 3), p(2 × 4), and p(4 × 2). We found that while u-Bri₁₊₄ or u-Bri₁₊₃ were the most stable, the relative stabilities of the different local minima structures varied with supercell size and shape. We found that for individual supercells the variation in energy between different local minima structures is on the order of 0.5 eV, but the variation in calculated formation energy for a specific structure depending upon supercell is up to 1 eV. Even omitting the two smallest supercells, often used in DFT studies, the variation with supercell size was around 0.8 eV, indicating that for oxygen vacancies on ceria(110) errors due to finite supercell sizes are larger than the variation with localization configuration, and can qualitatively affect the results of a calculation. We then assessed the scale of the remaining supercell size errors, and found that for some structures they remain on the 1 eV scale, indicating that the results for lone/low concentrations of vacancies may be different again. Indeed, we see also suggestions that for lone vacancies the optimal structure may even be s-Bri₃₊₄, NNN+NNN only localization, as seen for the (111) surface.^{7,10} Plausibly, this could also be true even for high concentrations of vacancies when they are randomly distributed.

We believe that there is little particularly special about the example chosen, so the general conclusion for defect calculations in metal oxides is that for the supercells commonly used in the literature, supercell (or indeed cluster) size related errors can both qualitatively and quantitatively affect predicted ground state and higher energy structures, and introduce errors in formation energies of isolated vacancies on the order of eV, even (as here) for neutral defects. Careful assessment of these errors in most individual cases is therefore required.

To summarize:

- We find three different geometrical structures for the oxygen vacancy on ceria (110), combined with many different Ce(III) localization patterns.
- The ground-state with most of the supercells studied here – an unsymmetric bridge structure with Ce(III) localization at NN and NNN positions – has not been found before.
- We see localisation at Ce sites that are NN+NNN coordinated to the vacancy, but speculative results from finite size scaling suggest that in the lone vacancy limit the coordination may be NNN+NNN only.

- The differences in formation energy due to the choice of supercell are on the same order as those due to the re-ordering of the Ce(III) ions around the vacancies, or larger.
- Even in p(3 × 3), errors in formation energies are up to ~1 eV, compared to lone vacancies.

ACKNOWLEDGMENTS

The authors would like to acknowledge the Swedish Foundation for International Cooperation in Research and Higher Education (STINT) and the Swedish Research Council (VR) for financial support and the Swedish Infrastructure for Computing (SNIC) for computing resources. Funding from the National Strategic e-Science program eSENCE is also gratefully acknowledged.

- ¹H. Nörenberg and G. A. D. Briggs, *Phys. Rev. Lett.* **79**, 4222 (1997).
- ²K. Fukui, Y. Namai, and Y. Iwasawa, *Appl. Surf. Sci.* **188**, 252 (2002).
- ³Y. Namai, K. Fukui, and Y. Iwasawa, *Catal. Today* **85**, 79 (2003).
- ⁴Y. Namai, K. Fukui, and Y. Iwasawa, *J. Phys. Chem. B* **107**, 11666 (2003).
- ⁵F. Esch, S. Fabris, L. Zhou, T. Montini, C. Africh, P. Fornasiero, G. Comelli, and R. Rosei, *Science* **309**, 752 (2005).
- ⁶J.-F. Jerratsch, X. Shao, N. Nilius, H.-J. Freund, C. Popa, M. V. Ganduglia-Pirovano, A. M. Burrow, and J. Sauer, *Phys. Rev. Lett.* **106**, 246801 (2011).
- ⁷M. V. Ganduglia-Pirovano, J. L. F. Da Silva, and J. Sauer, *Phys. Rev. Lett.* **102**, 026101 (2009).
- ⁸J. C. Conesa, *Catal. Today* **143**, 315 (2009).
- ⁹C. Zhang, A. Michaelides, D. A. King, and S. J. Jenkins, *Phys. Rev. B* **79**, 075433 (2009).
- ¹⁰H. Y. Li, H. F. Wang, X.-Q. Gong, Y.-L. Guo, Y. Guo, G. Lu, and P. Hu, *Phys. Rev. B* **79**, 193401 (2009).
- ¹¹T. X. T. Sayle, S. C. Parker, and C. R. A. Catlow, *Surf. Sci.* **316**, 329 (1994).
- ¹²T. X. T. Sayle, S. C. Parker, and C. R. A. Catlow, *J. Chem. Phys.* **98**, 13625 (1994).
- ¹³J. C. Conesa, *Surf. Sci.* **339**, 337 (1995).
- ¹⁴S. Vyas, R. W. Grimes, D. H. Gay, and A. L. Rohl, *J. Chem. Soc., Faraday Trans.* **94**, 427 (1998).
- ¹⁵M. Baudin, M. Wójcik, and K. Hermansson, *Surf. Sci.* **468**, 51 (2000).
- ¹⁶S. Gennard, F. Cora, C. Richard, and A. Catlow, *J. Phys. Chem. B* **103**, 10158 (1999).
- ¹⁷N. V. Skorodumova, M. Baudin, and K. Hermansson, *Phys. Rev. B* **69**, 075401 (2004).
- ¹⁸Z. Yang, K. Woo, M. Baudin, and K. Hermansson, *J. Chem. Phys.* **120**, 7741 (2004).
- ¹⁹M. Nolan, S. Parker, and G. W. Watson, *Surf. Sci.* **595**, 223 (2005).
- ²⁰S. Fabris, G. Vicario, G. Balducci, S. Gironcoli, and S. Baroni, *J. Phys. Chem. B* **109**, 22860 (2005).
- ²¹Y. Jiang, J. B. Adams, and M. van Schilfgaarde, *J. Chem. Phys.* **123**, 064701 (2005).
- ²²M. Nolan, S. Grigoleit, D. C. Sayle, S. C. Parker, and G. W. Watson, *Surf. Sci.* **576**, 217 (2005).
- ²³M. Nolan, S. C. Parker, and G. W. Watson, *Phys. Chem. Chem. Phys.* **8**, 216 (2006).
- ²⁴M. Nolan, S. C. Parker, and G. W. Watson, *Surf. Sci.* **600**, L175 (2006).
- ²⁵M. A. Henderson, C. L. Perkins, M. H. Engelhard, S. Thevuthasan, and C. H. F. Peden, *Surf. Sci.* **526**, 1 (2003).
- ²⁶M. V. Ganduglia-Pirovano, A. Hofmann, and J. Sauer, *Surf. Sci. Rep.* **62**, 219 (2007).
- ²⁷D. N. Belton and S. J. Schmieg, *J. Vac. Sci. Technol. A* **9**, 1416 (1991).
- ²⁸D. R. Mullins, S. H. Overbury, and D. R. Huntley, *Surf. Sci.* **409**, 307 (1998).
- ²⁹L. A. J. Garvie and P. R. Buseck, *J. Phys. Chem. Solids* **60**, 1943 (1999).
- ³⁰T. Holstein, *Ann. Phys.* **8**, 325 (1959).
- ³¹L. Friedman and T. Holstein, *Ann. Phys.* **21**, 494 (1963).
- ³²D. Emin and T. Holstein, *Ann. Phys.* **53**, 439 (1969).
- ³³B. Herschend, M. Baudin, and K. Hermansson, *Surf. Sci.* **599**, 173 (2005).

- ³⁴A. Gotte, K. Hermansson, and M. Baudin, *Surf. Sci.* **552**, 273 (2004).
- ³⁵N. M. Galea, D. O. Scanlon, B. J. Morgana, and G. W. Watson, *Mol. Simul.* **35**, 577 (2009).
- ³⁶Z. Yang, Z. Fu, Y. Wei, and K. Hermansson, *Chem. Phys. Lett.* **450**, 286 (2008).
- ³⁷Z. Yang, X. Yu, Z. Lu, S. Li, and K. Hermansson, *Phys. Lett. A* **373**, 2786 (2009).
- ³⁸C. W. M. Castleton and S. Mirbt, *Phys. Rev. B* **70**, 195202 (2004).
- ³⁹C. W. M. Castleton and S. Mirbt, *Phys. Rev. B* **73**, 035215 (2006).
- ⁴⁰R. Nieminen, *Modell. Simul. Mater. Sci. Eng.* **17**, 084001 (2009).
- ⁴¹C. W. M. Castleton, A. Höglund, and S. Mirbt, *Modell. Simul. Mater. Sci. Eng.* **17**, 084003 (2009).
- ⁴²C. Freysoldt, J. Neugebauer, and C. G. Van der Walle, *Phys. Rev. Lett* **102**, 016402 (2009).
- ⁴³G. Kresse and J. Hafner, *Phys. Rev. B* **49**, 14251 (1994).
- ⁴⁴G. Kresse and J. Furthmüller, *Comput. Mater. Sci.* **6**, 15 (1996).
- ⁴⁵S. L. Dudarev, G. A. Button, S. Y. Savrasov, C. J. Humphreys, and A. P. Sutton, *Phys. Rev. B* **57**, 1505 (1998).
- ⁴⁶J. P. Perdew, K. Burke, and M. Ernzerhof, *Phys. Rev. Lett.* **77**, 3865 (1996).
- ⁴⁷C. Loschen, J. Carrasco, K. M. Neyman, and F. Illas, *Phys. Rev. B* **75**, 035115 (2007).
- ⁴⁸D. A. Andersson, S. I. Simak, B. Johansson, I. A. Abrikosov, and N. V. Skorodumova, *Phys. Rev. B* **75**, 135109 (2007).
- ⁴⁹J. L. F. Da Silva, M. V. Ganduglia-Pirovano, J. Sauer, V. Bayer, and G. Kresse, *Phys. Rev. B* **75**, 045121 (2007).
- ⁵⁰C. W. M. Castleton, J. Kullgren, and K. Hermansson, *J. Chem. Phys.* **127**, 244704 (2007).
- ⁵¹P. E. Blöchl, *Phys. Rev. B* **50**, 17953 (1994).
- ⁵²N. A. Deskins, R. Rousseau, and M. Dupuis, *J. Phys. Chem. C* **115**, 7562 (2011).
- ⁵³C. Kanai, Y. Shichibu, K. Watanabe, and Y. Takakuwa, *Phys. Rev. B* **65**, 153312 (2002).
- ⁵⁴L. V. Pourovskii, A. V. Ruban, B. Johansson, and I. A. Abrikosov, *Phys. Rev. Lett.* **90**, 026105 (2003).
- ⁵⁵A. H. Höglund, C. W. M. Castleton, M. Götelid, B. Johansson, and S. Mirbt, *Phys. Rev. B* **74**, 075332 (2006).
- ⁵⁶G. Makov and M. C. Payne, *Phys. Rev. B* **51**, 4014 (1995).